Organic Electronics 67 (2019) 128–135

Contents lists available at ScienceDirect

Organic Electronics

journal homepage: www.elsevier.com/locate/orgel

Effects of thermally cross-linkable polymeric additive in the photoactive layer of polymer solar cells

Fang-Chi Hsu*, Jia-Yu Lin

Department of Materials Science and Engineering, National United University, Miaoli 360, Taiwan

ARTICLE INFO

Keywords:
Bulk heterojunction
Morphology
Stability
Crosslinking
GISAXS
Polymer solar cell

ABSTRACT

Performance and stability are the most important issues to be considered to propel and advance the polymer solar cell (PSC) technology to be realized in commercial market. Herein, we propose a new concept of stabilizing polymer-fullerene morphology for PSCs and simultaneously improve device performance by introducing thermally cross-linkable polymer as an additive in the photoactive layer. The cross-linker, poly[9,9-bis(6-(N,N-diethylamino)propyl)-fluorene-alt-9,9-bis(3-ethyl(oxetane-3-ethyloxy)hexyl)-fluorene] (PFN-ox), forms a three-dimensional network embedded in the polymer blend after thermal treatment and plays various roles including reducing the carrier recombination at the donor/acceptor interface, improving the electrical property of PSCs, enhancing the hydrophobicity of the photoactive layer, slightly decreasing fullerene domain size, and retarding the crystal growth of fullerenes. Those characteristics lead to the improvement of device performance from the moderate improved fill factor and stable device operation under ambient condition (> 85% efficiency retention after 2 months). The stability effects of PFN-ox are not only valid in polymer-fullerene blends, but also in polymer-polymer systems, showing its general characteristics. We believe that our finding can advance the development of stable PSCs and other optoelectronic devices based on organic materials.

1. Introduction

Polymer solar cells (PSCs) have gained considerable attention over the past few years for their advantages of processing simplicity, physical semi-transparency, mechanical flexibility, and light weight [1–4]. Typically, the photoactive layer of a PSC device is composed of a blend of a p-type conjugated polymer and an n-type acceptor, forming a bulk heterojunction (BHJ) structure. Significant progress in developing PSCs has been made with power conversion efficiency (PCE) over 10% for single junction cells based on the most promising BHJ architecture [5–7]. Still, these values are not sufficiently high to realize the application of PSCs in the market.

Recently, in addition to improving the PCE, device stability has been recognized as another important issue for commercializing PSCs. A number of studies have shown the detrimental effects of oxygen and moistures on device performance and the degradation mechanism of the photoactive layer involving chemical reaction are proposed [8–10]. To date, emerging stradegies for improving the device stability include the use of high-work-function metals as electrodes to avoid unwanted chemical oxidation [11,12], incorporating materials that can form either cross-linking or hydrogen bonding in the photoactive layers to stabilize the blend morphology, etc. [13–22]. Careful studies of these approaches are necessary in order to obtain stable polymeric solar cells. Among those stradegies, the idea of stabilizing morphology is to freeze the BHJ mixing result at the nanoscale, which is quite challenge. A potential solution of adopting the cross-linking concept; i.e., linking molecules by covalent bonds, appears to be promising to avoid molecular diffusion in the BHJ. Attempts to cross-linking either donor or acceptor molecules by careful design of cross-linkable moieties on polymers or fullerene derivatives have been successfully demonstrated [13–21]. Though the results are positive, the sysnthesis of customized polymers or fullerene-derivatives is time-consuming. Later on, a few groups have introduced low cost, easy attainable cross-linkers as additives in BHJ to cross-link polymer or fullerene derivatives under the irradiation of UV light [13,14,22–24] and the outcomes are also attractive. Among those low cost, easy attainable cross-linkers, the use of semiconducting polymer as the third component cross-linker in BHJ layer has not been seen in the literature yet.

Poly[9,9-bis(6-(N,N-diethylamino)propyl)-fluorene] (PFN), a conjugated polymer, has served as an interlayer in polymer light emitting devices to improve electron injection [25,26] and polymer solar cells to enhance electron extraction [27,28]. Its derivative, poly[9,9-bis(6′-(N,N-diethylamino)propyl)-fluorenealt-9,9-bis-(3-ethyl(oxetane-3-ethyloxy)-hexyl)-fluorene] (PFN-ox), with thermally crosslinkable property

* Corresponding author.
E-mail address: fangchi@nuu.edu.tw (F.-C. Hsu).

https://doi.org/10.1016/j.orgel.2019.01.024
Received 27 August 2018; Received in revised form 15 January 2019; Accepted 15 January 2019
Available online 17 January 2019
1566-1199/ © 2019 Elsevier B.V. All rights reserved.

has also gained attention for the fabrication of inverted solar cells for its insoluble characteristic after cross-linked [28–30]. Recently, several groups have tried to prepare electron transport layer of perovskite solar cells utilizing ZnO nanoparticles [31] and those commonly used acceptor materials for PSCs such as poly{[N,N′-bis(2-octyldodecyl)-1,4,5,8-naphthalene diimide-2,6-diyl]-alt-5,5'-(2,2'-bithiophene)} (N2200) [32] and (6,6)-phenyl C61 butyric acid methyl ester ($PC_{61}BM$) [33] mixed with a small amount of PFN-ox. Those hybrid acceptor-PFN-ox electron transporting layers can facilitate their electron transporting properties and enhance as well as stabilize the ambient device operation. Though PFN-ox has been successfully demonstrated its promising potential as an electron transport layer, the incorporating of PFN-ox into the BHJ photoactive layer of PSCs has not been seen in the literature yet.

In this paper, we propose a new concept of stabilizing polymer-fullerene morphology and simultaneously improve the resulting device performance by introducing a thermally cross-linkable polymer PFN-ox as an additive in the photoactive layer of PSCs. To carry out the idea, we choose the well-known conjugated polymer, poly(3-hexythiophene (P3HT), blended with $PC_{61}BM$ as the model system for demonstration and fundamental mechanism study. After annealing the BHJ layer at 120 °C for 20 min, PFN-ox forms a three-dimensional network in the BHJ such that the blend film does not rapidly redissolved in its processing solvent and the surface of the film becomes more hydrophobic. We compare the performance and the stability of devices containing various amounts of PFN-ox. It is found that the incorporation of PFN-ox enhances both the carrier dynamics and the electrical properties of the devices, resulting in an improved PCE from a moderate enhanced fill factor (*FF*) and subtle improved open circuit voltage (V_{oc}). For the stability study, those cross-linked devices show long-term stable operation in the air, which can be attributed to the improved hydrophobicity of the BHJ films and the retarded fullerene aggregation in the presence of rigid PFN-ox network. Those promising properties are also observed in high performance polymer-fullerene and all polymer BHJ systems, showing the general application of PFN-ox.

2. Experimental section

2.1. Material preparation

ZnO nanoparticles were synthesized according to Ref. [34]. Initially, 440 mg of zinc acetate dihydrate ($Zn(CH_3COO)_2 \cdot 2H_2O$) powder was dissolved in 20 mL of ethanol. Then, 116 mg of lithium hydroxide monohydrate ($LiOH \cdot H_2O$) was added into the previous solution followed by 30 min ultrasonic bath. After the solution turned clear, 0.4 mL of DI water was then added and stirred at 500 rpm, 60 °C in water bath to complete the reaction. The synthesized ZnO nanoparticles were then collected by centrifuging the resulting solution. The ZnO nanoparticle solution was prepared by re-dispersing 15 mg of the collected nanoparticles in 1 mL of isopropanol. Photoactive materials including P3HT, $PC_{61}BM$, $PC_{71}BM$, and PFN-ox were purchased commercially from Lumtech Inc. While poly[(2,6-(4,8-bis(5-(2-ethylhexyl)thiophen-2-yl)-benzo[1,2-b:4,5-b']dithiophene))-alt-(5,5-(1',3'-di-2-thienyl-5',7'-bis(2-ethylhexyl)benzo[1',2'-c:4',5'-c']dithiophene-4,8-dione))] (PBDBT) and poly[[N,N′-bis(2-octyldodecyl)-naphthalene-1,4,5,8-bis(dicarboximide)-2,6-diyl]-alt-5,5′-(2,2′-bithiophene)] (N2200) were obtained from Solarmer Inc. and Polyera Inc., respectively. All materials were used as received.

2.2. Device preparation

Indium tin oxide (ITO)-patterned glass substrates (15 Ω/□) were cleaned by successive sonication in commercial wafer cleaning buffer solution, acetone and isopropanol and then dried in N_2 gas flow before used. An ~30 nm thick ZnO film was deposited by spin-coating the prepared nanoparticle solution on the cleaned ITO glass substrates. Mixture of 20 mg of P3HT and 20 mg of $PC_{61}BM$ in 1 mL of o-dichlorobenzene (ODCB) was stirred at 500 rpm, 60 °C on a hot plate for one day. PFN-ox in a weight fractions of 0, 0.5, 1, 3, 5, and 7% of donor and acceptor were added into the previous mixture, respectively. For PBDBT based BHJ blend solutions, PBDBT:$PC_{71}BM$ (D/A ratio 1:1) and PBDBT:N2200 (D/A ratio 3:1) were prepared with concentrations of 16 and 12 mg mL^{-1}, respectively. The former one was in chlorobenzene (CB) and the latter one was in a mixed solvent of CB and 2-Methyltetrahydrofuran (MeTHF) (2.5:1 v/v). The reason we use cosolvent for preparing PBDBT:N2200 solution is because N2200 dissolves better in MeTHF with more oriented polymer chain arrangement than in CB [35,36]. Therefore, we choose a mixed solvent approach. Both types of solutions were stired at 85 °C for 8 h and no processing additive was added. In these PBDBT based blend solutions, only 3% of PFN-ox was introduced. The blend solutions were then spin-coated onto the ZnO films at 700 rpm for 1 min followed by vacuum dry and thermal treatment at 120 °C for 20 min in a N_2-filled environment. We had tried to examine the cross-linked time for PFN-ox and it took around 20 min for it to fully cross-linked (see Fig. S1, Supplementary Information). Those P3HT:$PC_{61}BM$, PBDBT:$PC_{71}BM$, and PBDBT:N2200 photoactive films were ~150, ~100, and ~85 nm thick, respectively, to serve as the light absorbing layers. Finally, MoO_3 (7 nm) and Ag (100 nm) layers were deposited in order on those light absorbers to complete the solar cell device fabrication. The active area of the finished devices defined by the overlapping of ITO and Ag electrodes was 0.04 cm^2.

2.3. Characterization details

The optical absorption spectra were collected by using a Shimadzu Model UV-2600 UV–vis spectrophotometer. Surface morphology images were taken by using an atomic force microscopy (AFM, Digital Instruments, Nanoscope III). The contact angle values were measured by a contact angle/surface tension analyzer (FTA-125). The current density – voltage (*J* – V) characteristics of solar cells were evaluated by using a Keithley Model 2410 source meter under irradiation intensity of 100 mW/cm^2 from a calibrated solar simulator (Newport Inc.) with an AM 1.5G filter. The calibration was done by using a standard Si photodiode. The incident-photon-conversion-efficiency (IPCE) spectra were recorded using a setup composed of a lamp system (Newport Inc.), a chopper, a monochromator, a lock-in amplifier, and a standard silicon photodetector (ENLI Technology). Impedance spectroscopy (IS) was conducted by a Zahner electrochemical workstation Model Zennium with an ac voltage of 20 mV over a frequency range from 100 to 4 MHz at short circuit condition under irradiation intensity of 100 mW/cm^2 from a calibrated solar simulator (Newport Inc.) with an AM 1.5G filter. Grazing-incidence small-angle X-ray scattering (GISAXS) measurements were performed at the 23A beamline (10 keV) of the National Synchrotron Radiation Research Center (NSRRC), Hsinchu, Taiwan, using a 0.2° incident angle. The thickness of the film was measured by AMBIOS Technology Model XP-2 surface profilometer.

3. Results and discussion

3.1. BHJ film properties

Fig. 1 illustrates the inverted device structure (ITO/ZnO/photoactive layer/MoO_3/Ag) and the chemical structures of materials used in this study. P3HT and PBDBT are polymer donors while $PC_{61}BM$, $PC_{71}BM$, and N2200 serve as acceptors. Three kinds of photoactive layers including P3HT:$PC_{61}BM$, PBDBT:$PC_{71}BM$, and PBDBT:N2200 are prepared for this study. PFN-ox [29,30] is the thermally crosslinkable polymeric additive in the photoactive layers. Throughout this article, as-prepared film denotes the annealing-free photoactive layer, but otherwise annealed at 120 °C for 20 min or as noted.

Fig. 2 presents the water contact angle results for as-prepared P3HT:$PC_{61}BM$ (0(as-prepared)) film and the associated annealed ones

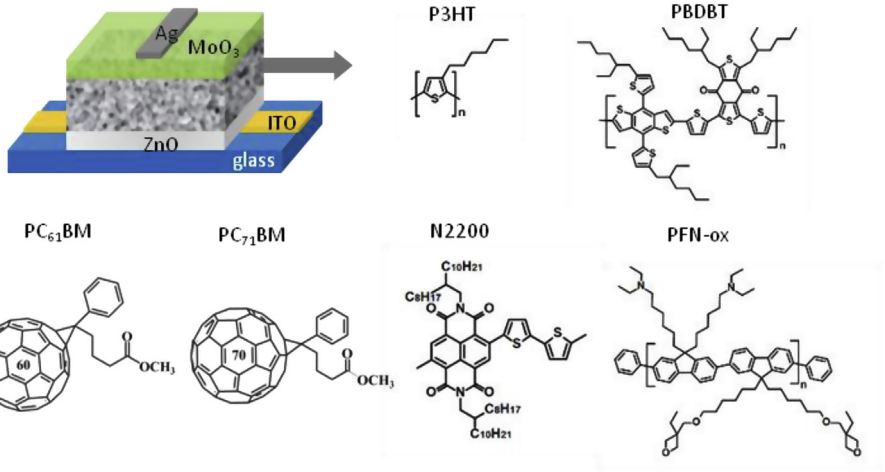

Fig. 1. Device structure along with the chemical structures of materials used in the photoactive layer.

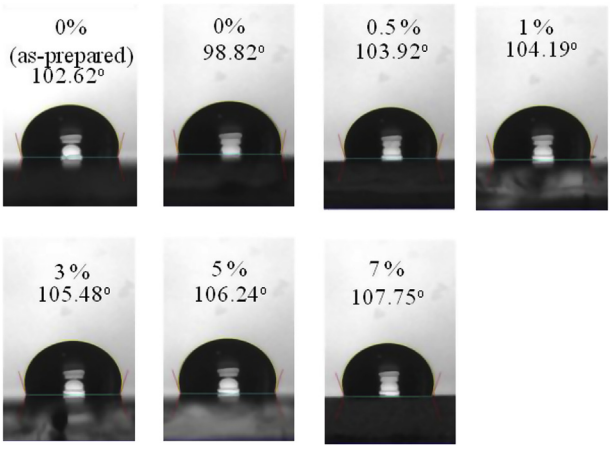

Fig. 2. Water contact angle measurement results of as-prepared P3HT:PCBM film and the associated annealed ones containing PFN-ox of 0, 0.5,1, 3, and 5, and 7%.

containing 0, 0.5, 1, 3, 5, and 7% PFN-ox deposited on glass substrates. After heat treatment, the contact angle value for the as-prepared P3HT:PC_{61}BM film (0%) was reduced. By adding PFN-ox, the angle became larger and the value increased with the increased amount of the cross-linker, suggesting an enhanced hydrophobicity of the film surface in the presence and with the amount of the cross-linker.

Fig. 3 displays the topographic images of various P3HT:PC_{61}BM films deposited on ZnO by using AFM. All those films show similar surface features. The root-mean-square (r.m.s.) surface roughness values are 5.26, 4.58, 2.92, 3.09, 3.29, 3.45, and 3.9 nm for films containing 0 (as-prepared), 0, 0.5, 1, 3, 5, and 7% PFN-ox, respectively. The surface of the as-prepared P3HT:PC_{61}BM film is relatively smooth after thermal treatment. With the addition of PFN-ox, all the films are even smoother and the r.m.s. values increase with additive concentration, indicating that PFN-ox can improve the interface compability between polymer and fullerene at different extent. We have tried to study the morphologies of annealed films containing 0 and 3% PFN-ox using transmission electron microscopy (TEM). According to TEM images, these two films exhibit different extent of phase separation (Fig. S2, Supplementary Information). The PC_{61}BM-rich domain in P3HT:PC_{61}BM:PFN-ox film is relatively smaller due to better mixing, a result which supports AFM finding.

To gain more insights of PFN-ox network in BHJ, GISAXS measurements were performed for samples containing 0 and 3% PFN-ox. Fig. 4 (a–d) present the 2-D GISAXS images of P3HT:PC_{61}BM films in as-prepared and annealed conditions as well as blend films containing 3% PFN-ox prepared in the same conditions. Fig. 4e displays the line-cut 1-D profiles of these images along the in-plane direction (the rectangular regions). We deducted these 1-D profiles from the background of the blank silicon wafer. The PC_{61}BM cluster sizes for these four conditions can be determined by fitting the GISAXS profiles (see Supplementary Information for details). The fits yielded the mean PC_{61}BM cluster sizes of 18.0 and 18.8 nm for P3HT:PC_{61}BM blend films before and after thermal annealing, respectively. For samples incorporating 3% PFN-ox, the mean cluster sizes were reduced to 14.8 and 16.6 nm in as-prepared and annealed conditions, respectively. Therefore, the presence of PFN-ox slightly reduces the fullerene cluster size and the size increases after heat treatment.

For the optical properties, the introduction of PFN-ox into P3HT:PC_{61}BM neither alters the absorption characteristics nor the intensity of the pristine BHJ film, an indication of negligible photon absorption contributed from PFN-ox. However, if we compare the spectra for the same film, after annealing, it clearly shows that two signature peaks of P3HT at 550 and 610 nm become slightly intensified due to an

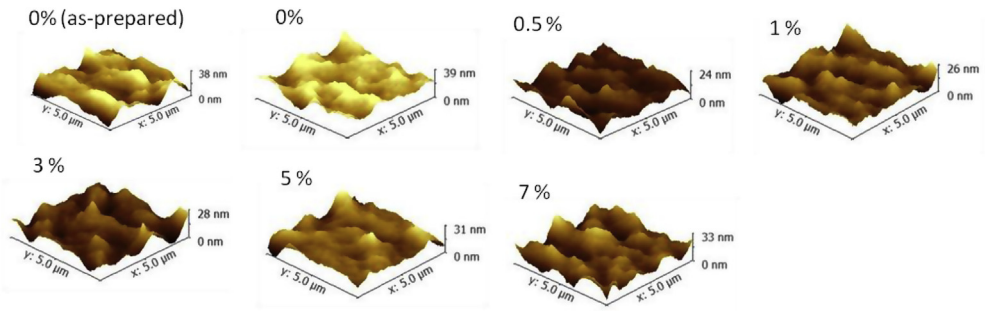

Fig. 3. AFM images of 5 µm × 5 µm surface area of as-prepared P3HT:PCBM film and the associated annealed ones containing PFN-ox of 0, 0.5,1, 3, and 5, and 7%.

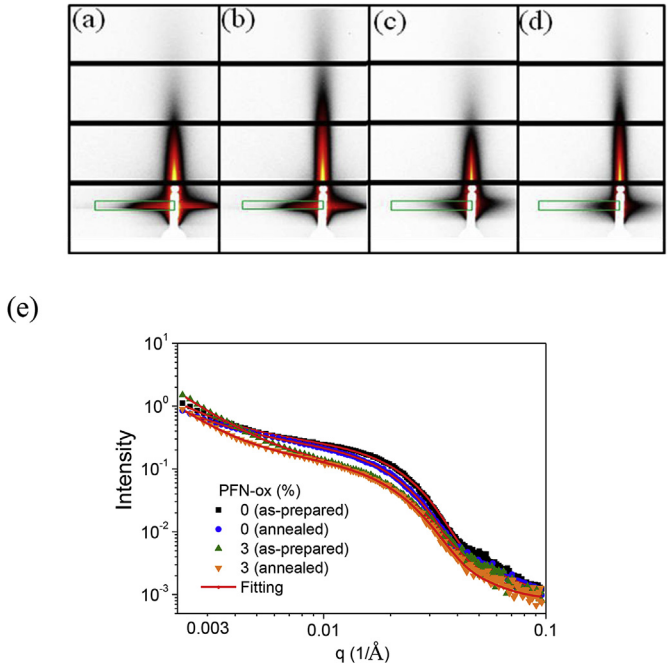

Fig. 4. 2-D GISAXS patterns of (a) as-prepared and (b) annealed P3HT:$PC_{61}BM$ blend films as well as the blend films containing 3% PFN-ox in (c) as-prepared and (d) annealed conditions. (e) Line-cut 1-D profiles of (a–d) images along the in-plane direction (the rectangular regions).

enhanced interchain interaction (Fig. S3, Supplementary Information). Therefore, PFN-ox network in the BHJ film still allows polymer chain moving for better ordering.

3.2. Device performance

We then evaluated the device performance selectively made from those films. Fig. 5a shows the current density (J) – voltage (V) curves for the best P3HT:$PC_{61}BM$ devices containing various amounts of PFN-ox. The corresponding device performance parameters by taking the average over 10 cells are summarized in Table 1. The performance of as-prepared P3HT:$PC_{61}BM$ device is comparable with literature reports [37,38] and the thermally treated cell also shows similar performance. Introducing PFN-ox into the photoactive layer leads to the improvement of device performance. The optimum concentration of PFN-ox was found to be 3 wt% of the total weight of P3HT and $PC_{61}BM$, resulting in an approximately 14% increment in PCE from 3.28% to 3.74% for the best device due to subtle improved open circuit voltage (V_{oc}) and moderate enhanced fill factor (*FF*) while the short circuit density (J_{sc}) remained similar. The integrated J_{sc} values obtained from the IPCE spectra were 9.63, 9.49, 9.36, 9.50, and 9.25 mA/cm^2 for devices containing 0 (as-prepared), 0, 0.5, 3, and 7% PFN-ox, respectively (Fig. 4b), in good aggrement with the current obtained from J–V measurements and confirming the similarity of J_{sc} values for all devices.

3.3. Charge transport study

To understand the device improvement in the presence of PFN-ox, we studied the charge transfer dynamics and recombination processes at the interfaces of those devices by performing impedance spectroscopy (IS). Those devices were probed in response to an ac perturbation of 20 mV varied over a frequency range from 100 to 4 MHz. Fig. 6 shows the Nyquist plots of P3HT:$PC_{61}BM$ devices containing 0 (as-prepared), 0, and 3% PFN-ox measured at zero dc bias under one sun condition and the results were fitted using the equivalent circuit model shown in Supplementary Information Fig. S4. The intercept of the semicircle with the lateral axis at low frequency carries the information of the recombination (R_{rec}) resistances [39]. The R_{rec} values obtained from each semicircle were 2.53, 2.57, 3.58 KΩ for BHJ containing 0 (as-prepared), 0, and 3% PFN-ox, respectively. The improved R_{rec} in the cross-linked film indicates that the probability for free carrier recombination through the donor-acceptor interface is reduced, a result which is also inferred by the carrier lifetime. The average carrier lifetime can be calculated from the frequency at the maximum height of the semicircle and the values are 8.30, 8.64, and 13.07 μs for 0 (as-prepared), 0, and 3% PFN-ox devices, respectively, suggesting a lengthened carrier lifetime in the cross-linked BHJ film. The underlying electrical parameters related to various physical processes were also extracted by the equivalent circuit model shown in Supplementary Information Fig. S4 along with the fitting results listed in Supplementary Information Table S1. The electrical parameters, including recombination resistance and the average carrier lifetime, estimated from the fits of the Nyquist plots are in agreement with the experimental data. The improved recombination resistance and carrier lifetime can account for the improvement in *FF* of the cross-linked devices.

From the engineering perspective, both the series resistance (R_s) amd the shunt resistance (R_{sh}) determine the value of *FF*. As summarized in Table 1, after incorporating PFN-ox, R_s decreases slightly whereas there is a substantial enhancement in R_{sh}, for example, ~20% increment for 3% PFN-ox. The improved R_s and R_{sh} may be due to a smoother BHJ film surface forming better electrical contact with the thin MoO_3 and Ag layers, which can prevent Ag nanoparticles from direct contacting or diffusing into BHJ during thermal deposition. Both the improvement in R_s amd R_{sh} can also contribute to the improved *FF*.

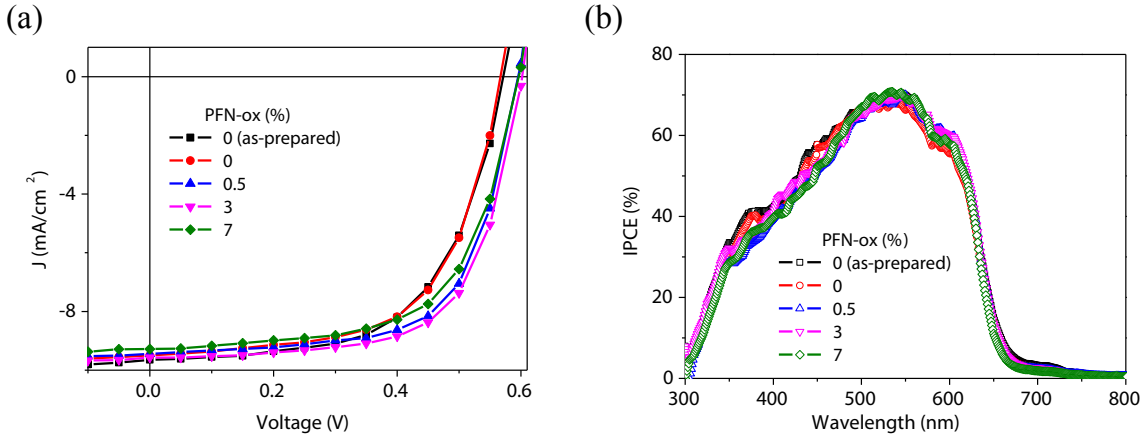

Fig. 5. (a) J-V characteristics and (b) IPCE spectra of devices with 0, 0.5, 3, and 7% PFN-ox.

Table 1
Summary of device performance parameters under one sun condition with AM 1.5G filter. The values in the parenthesis denote the values for the best device.

PFN-ox (%)	J_{sc} (mA/cm^2)	V_{oc} (V)	*FF* (%)	*PCE* (%)	*Rs* (Ωcm^2)	R_{sh}(Ωcm^2)
0 (as-prepared)	9.49 ± 0.17 (9.65)	0.57 ± 0.01 (0.57)	60.51 ± 0.88 (59.55)	3.27 ± 0.11 (3.28)	(9.28)	(1069)
0	9.44 ± 0.39 (9.5)	0.57 ± 0.01 (0.57)	59.15 ± 0.67 (60.79)	3.20 ± 0.09 (3.27)	(9.87)	(1090)
0.5	9.38 ± 0.15 (9.44)	0.60 ± 0.00 (0.60)	65.51 ± 0.17 (65.23)	3.67 ± 0.05 (3.66)	(7.79)	(1282)
3	9.49 ± 0.08 (9.57)	0.60 ± 0.00 (0.60)	65.84 ± 0.42 (65.39)	3.75 ± 0.02 (3.74)	(7.65)	(1293)
7	9.24 ± 0.08 (9.27)	0.60 ± 0.00 (0.60)	63.15 ± 0.26 (63.00)	3.47 ± 0.03 (3.48)	(8.71)	(1096)

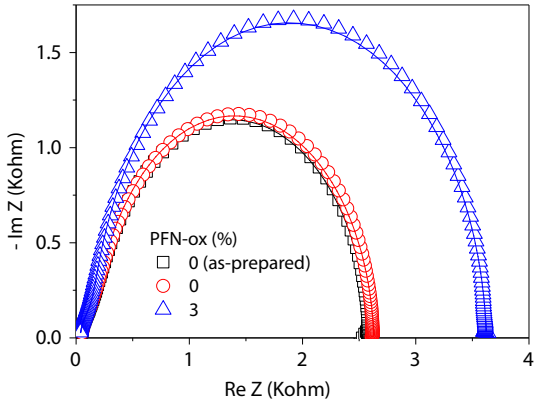

Fig. 6. Nyquist plot for P3HT:PCBM films containing 0 and 3% PFN-ox and the solid lines are the fitting curves.

We also measured the electron and the hole mobilities of those BHJ films using space-charge-limited-current (SCLC) method. The structures of the electron- and the hole-only devices were ITO/ZnO/photoactive layer/Al and ITO/PEDOT:PSS/photoactive layer/MoO_3/Ag, respectively. The electron mobilities calculated from the fits in Fig. 7a were 7.3×10^{-5}, 8.0×10^{-5}, and 1.2×10^{-4} cm^2/V for P3HT:PC_{61}BM containing 0 (as-prepared), 0, and 3% PFN-ox, respectively, while the hole mobilities estimated from the fits in Fig. 7b were 5.5×10^{-5}, 5.6×10^{-5}, and 6.0×10^{-4} cm^2/V, respectively. The presence of PFN-ox can facilitate electrons transporting throughout the fullerene phase [33] and holes in the polymer phase. Based on the results, we calculated electron-to-hole mobility ratios and the result yielded 1.33, 1.43, and 1.97 for films containing 0 (as-prepared), 0, and 3% PFN-ox, respectively. The addition of PFN-ox leads to a slightly unbalanced charge transport configuration of the bi-continuous pathways, which can result in charge accumulation inside device and lower the photocurrent. Though IS measurements reveal the improvement in interfacial charge recombination property and carrier lifetime of cross-linked devices, the overall combination effect involving the mobility result may not yield a significant enhancement in J_{sc}.

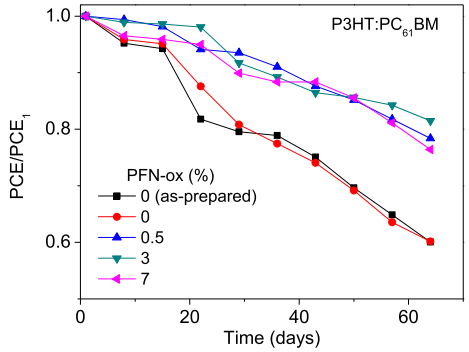

Fig. 8. Normalized PCEs for the ambient operation of P3HT:PC_{61}BM devices stored in the air for 2 months.

3.4. Stability study

The long-term stability of PSCs was examined for 2 months at room temperature in the laboratory environment. The $J - V$ curves of the test devices were periodically recorded. As shown in Fig. 8, the non-cross-linked devices retained 60% of their initial PCEs after 2 months, a result which is similar to that reported in the literature [40]. After incorporating PFN-ox, the cross-linked devices were relatively stable and retained 80% of their original PCEs. As mentioned in the introduction, there are several possible factors, including oxygen, moisture, and metals [8–10,40–42], can diffuse into the photoactive layer and degrade device performance. Since P3HT:PC_{61}BM films became more hydrophobic with the addition of PFN-ox as evidenced by the larger contact angle values, we would expect that the hydrophobic surface character can prevent the adsorption of water molecules in the air from diffusion into the photoactive layer laterally [40] and degrade the device.

3.5. Mechanism study for stability

It is known that semicrystalline polymers including P3HT tend to repel fullerene during crystallization upon post-annealing. This property enables to finely tune the polymer-fullerene BHJ morphology;

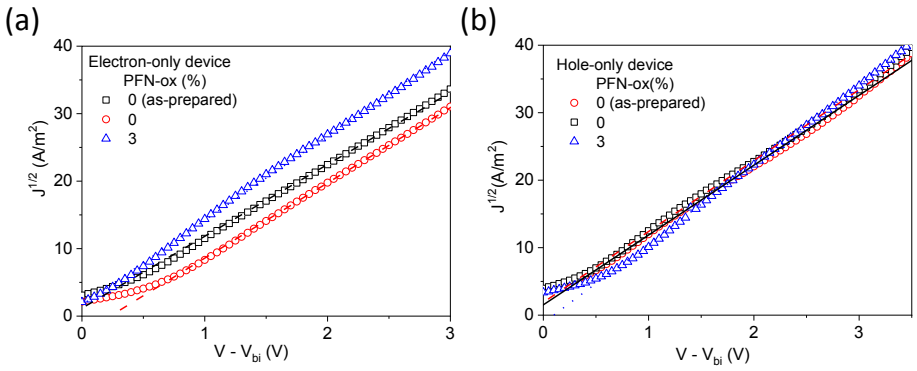

Fig. 7. $J^{1/2} - V$ characteristics of (a) the electron- and (b) the hole-only devices for as-prepared P3HT:PC_{61}BM film and the associated heat-treated films containing 0 and 3% PFN-ox of different thicknesses.

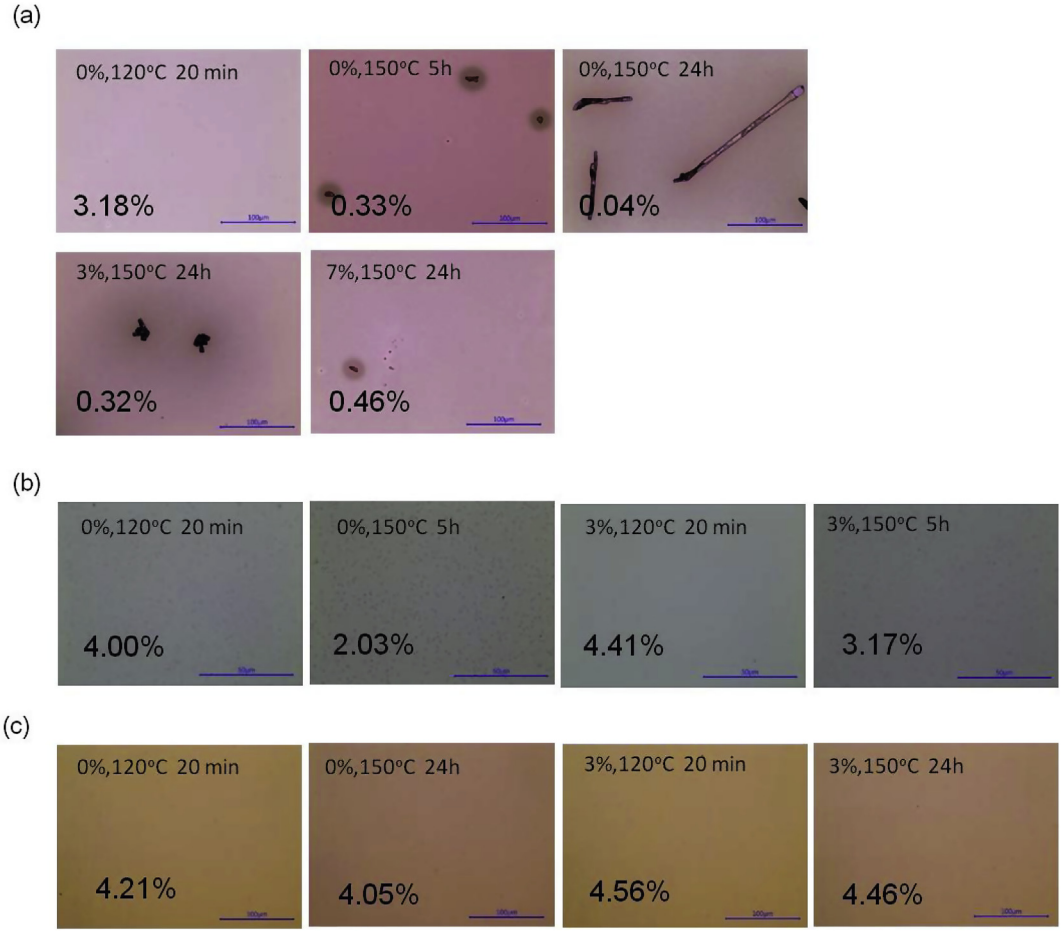

Fig. 9. Optical images for polymer blend films prepared at various conditions with the corresponding device PCEs noted. (a) As-prepared P3HT:$PC_{61}BM$ film and films containing 3 and 7% PFN-ox annealed at 120 °C for 20 min or at 150 °C for 5 or 24 h. (b) PBDBT:$PC_{71}BM$ films containing 0 and 3% PFN-ox annealed at 120 °C for 20 min and at 150 °C for 5 h. (c) PBDBT:N2200 containing 0 and 3% PFN-ox annealed at 150 °C for 24 h. The scale bar for (a) and (c) is 100 μm and it is 50 μm for (b).

however, the crystal growth is substantially increased with heating time. Explicitly, those semicrystalline polymer-fullerene blends are not stable because fullerene domains always tend to enlarge with time or upon heating leading to PCE loss [43]. Here, we study the thermal effects of PFN-ox on P3HT:$PC_{61}BM$. The photoactive layers were thermally annealed at 150 °C for an extended period of time and the corresponding surface images as well as the device performance were evaluated. As the optical image shown in Fig. 9a, micron-sized crystals of $PC_{61}BM$ were clearly visible after annealing for 5 h and the crystals grew with the heating time, i.e., > 100 μm for 24 h. Upon this heating process, devices exhibited significantly dropping of PCEs from 3.18% to 0.04%. Fortunately, the crystal growth was retarded by the introduction of PFN-ox. Higher PFN-ox amounts do freeze efficiently the BHJ morphology with less crystal growth and result in higher PCE. The effect of the suppression of $PC_{61}BM$ diffusion in the semicrystalline P3HT can contribute to the ambient operation stability of devices.

Considering the amorphous polymer-fullerene systems, fullerene crystals will certainly start growing with time due to Ostwald ripening [44] though there is a driving force to polymer reorganization. Conjugated polymer, PBDBT (Fig. 1), is a known donor material enabling outstanding PCEs over 10% [45]. PBDBT is a less crystalline polymer than P3HT and could result in smaller BHJ morphological features because the fullerene are better interpenetrated within the polymer [46]. As seen in Fig. 9b, after annealing 5 h at 150 °C, the aggregration of $PC_{71}BM$ becomes visible and homogenous in contrast to the micron-sized crystals produced in semicrystalline polymer matrix. The corresponding PCE drops to half of its initial value. Adding 3% PFN-ox reduces the aggregration of $PC_{71}BM$ and results in a slightly drop of PCE from 4.41% to 3.17%. Similarly, increasing PFN-ox concentration to 7% minimizes the visible aggregation of $PC_{71}BM$, and hence less PCE loss. The performance of PBDBT:$PC_{71}BM$ based devices prepared at 120 °C is provided in Supplementary Information Fig. S5 and Table S2. We have also checked the ambient operation of those devices and found that the cross-linked cells are indeed relatively stable (Fig. S6b, Supplementary Information) Our morphological stablization strategy of using thermally cross-linkable PFN-ox is effective in both semicrystalline- and amorphous-fullerene blends system to retard the diffusion of fullerene molecules.

To extend our approach to polymer-polymer blend, we investigated morphology stablization of all-polymer, PBDBT:N2200, system upon cross-linking. The performance of PBDBT:N2200 based devices prepared at 120 °C is summarized in Supplementary Information Fig. S5 and Table S3. As revealed by the optical microscope image (Fig. 9c), we did not observe any apparent micro-phase separation characteristics for the pristine and the cross-linked films even annealing up to 24 h and the corresponding PCEs of the devices remained similar to their initial values. We compared the ambient operation stability of those devices. After 30 days, the pristine PBDBT:N2200 device still retained ~84.5% of its original PCE (Fig. S6a, Supplementary Information). According to Zhang et al. [47], devices are more stable at higher PBDBT content. For examples, D:A ratios of 1:1 and 10:1 retained ~85% and 98% of their initial PCEs after 30 days, respectively. We prepared our devices in a D:A ratio of 3:1 and the slightly faster degradation of our devices may be due to our laboratory storage environment instead of using a glove

box as Zhang et al.'s work [47]. Fortunately, adding 3% PFN-ox into PDBDT:N2200 can effectively improve device stability for the retention of 86.1% of its initial PCE after the same period of time. Though there is no dramatic morphology difference, the superior ambient operation stability of cross-linked all-polymer PSCs over the pristine cell can be attributed to the more hydrophobic character of the BHJ with PFN-ox (see Fig. S7, Supplementary Information). We mention here that for all PBDBT based devices, we do not try to optimize their performance through adding typical processing additives or finding a proper thickness of the photoactive layer. Our purpose here is to study the physical phenomenon.

From the above studies, the introduction of thermally cross-linkable polymer PFN-ox as an additive in the polymer:fullerene photoactive layer of PSCs enhances device performance and stability. The enhancement in PCE comes from the moderate improvement in *FF* and subtle enhanced V_{oc}. In the presence of PFN-ox, the surface of BHJ becomes smoother, implying an improvement in compability between P3HT and $PC_{61}BM$. According to IS study, carrier recombination at the donor/acceptor interface is decreased resulting in higher recombination resistance and lengthened carrier lifetime. The improved interfacial carrier dynamics and electrical properties of the cross-linked devices lead to the enhancement in *FF*. It is reported [30,31,33] that PFN-ox has a strong doping effect on fullerene molecules, which enables a greater electron transport ability of the fullerene films. In a BHJ, it is found that the electron mobility in the fullerene phase is also improved and so does the hole mobility in the polymer phase. Unfortunately, the resulting charge transport property is slightly unbalanced and could lead to charge accumulation inside devices. The combination effect of the interface charge transport and the mobility studies may not result in an apparent improvement in J_{sc}. On the other hand, the strong electron transfer from PFN-ox onto fullerene can increase the carrier concentration in the fullerene phase and hence move its quasi Fermi level closer to LUMO. As a result, the quasi Fermi level difference between P3HT and $PC_{61}BM$ will be enlarged leading to improved V_{oc}.

Morphology stability of BHJ is important for the lifetime of solar cells. It is found that cross-linked films are more hydrophobic. The increased hydrophobicity of BHJ surface can prevent the adsorption and the subsequent diffusion of water molecules from the air and hence minimize the unexpected chemical/electrochemical degradation induced in the photoactive layer. Physically, PFN-ox can effectively retard the crystal growth of fullerene micro-domains in either semi-crystalline or amorphous polymer matrix. Higher amounts of PFN-ox exhibit a better ability to prevent fullerenes from diffusion in polymer matrix. As the schematic diagram of P3HT:$PC_{61}BM$ BHJ shown in Fig. 10, PFN-ox forms a three-dimensional network embedded in the BHJ with slightly reduced fullerene domain size as suggested by the GISAXS results and the degree of cross-linking depends on its concentration. At higher amount of PFN-ox, the rigid network becomes denser and thus, restricts fullerene diffusion. Thus, both the enhanced hydrophobicity and redarded fullerene diffusion properties induced by PFN-ox network lead to the improved device stability. And the effect should be independent of donor polymers chosen, including other high efficiency polymers, PffBT4T and PTB7-Th. Interestingly, PFN-ox also works effectively in all-polymer BHJ for extending the device lifetime due to the improved hydrophobilicity of the BHJ film (Fig. S7, Supplementary Information). Considering other nonfullenene acceptors such as ITIC, PBDBT:ITIC devices are shown to exhibit excellent thermal stabilities than PBDBT:$PC_{71}BM$ ones due to the relatively stable morphology in contrast to the formation of large $PC_{71}BM$ clusters in polymer-fullerene film [45]. Therefore, we would expect that PFN-ox has the same effect on the stability of polymer:ITIC system as polymer-polymer devices.

There are several advantages of using thermally cross-linkable PFN-ox as an additive in preparing the BHJ layer for PSCs. Mostly, the cross-linking reaction used in polymer-fullerene blends [13,14,16–24] is based on UV light initiation, which could introduce additional photo-degradation effect in the materials themselves. Thermal cross-linking process with mild temperature ~100 °C is more desirable because polymer chains can be reorganized without decomposition such that the blend morphology can be finely tuned. A proper nanomorphology of donors and acceptors can be achieved along with the completion of cross-linking, which benefits the device performance. From the cost-effective perspective, PFN-ox is commercially available, relatively inexpensive than its mother polymer PFN, readily to be incorporated in any BHJ blend, and having apparent effect in stabilizing device operation in ambient regardless of polymer-fullerene or polymer-polymer blend based PSCs. We believe that our finding for the new way of using PFN-ox can advance the development of stable and high performance PSCs.

4. Conclusions

We demonstrate a new concept of stabilizing polymer-fullerene morphology and simultaneously improve the resulting device performance through introducing of a thermally cross-linkable polymeric additive in the photoactive layer of PSCs. The additive PFN-ox cross-links and forms a three-dimensional network along with the fine tunning of the polymer blend nanomorphology upon heating at mild temperature (~120 °C). This type of cross-linking process is facile and allows the preparation of stable polymer BHJ formulations while fine tunning their nanomorphology. The resulting devices are of improved device performance, primarily from the improvement in *FF* and V_{oc} due to reduced charge recombination and improved electrical properties. Depending on the material properties of donor-accepter pair and the

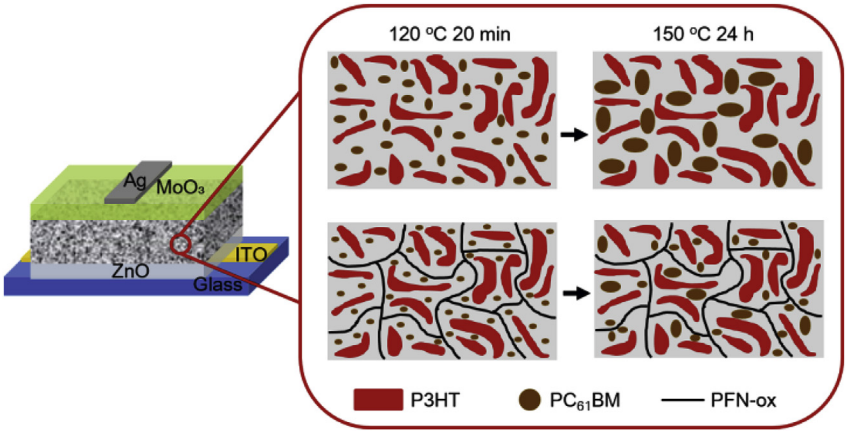

Fig. 10. The schematics of the BHJ structure containing 0 and 3% PFN-ox annealed at 120 °C for 20 min and at 150 °C for 24 h.

amount of cross-linkers, different stabilization extent of PCEs can be obtained, which could be optimized by further studies. The origin for ambient operation stability improvement can be attributed to the improved hydrophobicity of the photoactive layer for preventing water molecules diffusion from the air and the suppression of larger size fullerene crystallites in the polymer matrix. Our finding for the stability effect of PFN-ox on PSCs is general and it should be able to be generalized to other polymer based opto-electronic devices for improving the operation stability.

Acknowledgement

Authors would like to thank Prof. Yu-Wei Su from Department of Chemical Engineering at Fong-Jia University for the assistance of GISAXS measurement and data discussion. This work is supported by Ministry of Science and Technology, Taiwan (Project No. MOST 105 - 2112 - M − 239 - 001 - MY3).

Appendix A. Supplementary data

Supplementary data to this article can be found online at https://doi.org/10.1016/j.orgel.2019.01.024.

References

[1] G. Li, R. Zhu, Y. Yang, Polymer solar cells, Nat. Photon. 6 (2012) 153–161.
[2] Y. Liang, Z. Xu, J. Xia, S.T. Tsai, Y. Wu, G. Li, C. Ray, L. Yu, For the bright future—bulk heterojunction polymer solar cells with power conversion efficiency of 7.4%, Adv. Mater. 22 (2010) 135–161.
[3] H. Benten, D. Mori, H. Ohkita, S. Ito, Recent Research progress of polymer donor/polymer acceptor blend solar cells, J. Mater. Chem. 4 (2016) 5340–5365.
[4] Y. Li, C. Xu, C. Cui, Y. Li, Flexible and semitransparent organic solar cells, Adv. Energy Mater. 8 (2018) 170791.
[5] J. Zhao, Y. Li, G. Yang, K. Jiang, H. Lin, H. Ade, W. Ma, H. Yan, Efficient organic solar cells processed from hydrocarbon solvents, Nat. Energy. 1 (2016) 15027.
[6] Q. Wan, X. Guo, Z. Wang, W. Li, B. Guo, W. Ma, M. Zhang, Y. Li, 10.8% efficiency polymer solar cells based on PTB7-Th and PC71BM via binary solvent additives treatment, Adv. Funct. Mater. 26 (2016) 6635–6640.
[7] W. Zhao, D. Qian, S. Zhang, S. Li, O. Inganäs, F. Gao, J. Hou, Fullerene-free polymer solar cells with over 11% efficiency and excellent thermal stability, Adv. Mater. 28 (2016) 4737–4739.
[8] A. Seemann, H.J. Egelhaaf, C.J. Brabec, J.A. Hauch, Influence of oxygen on semi-transparent organic solar cells with gas permeable electrodes, Org. Electron. 10 (2009) 1424.
[9] T.S. Glen, N.W. Scarratt, H. Yi, A. Iraqi, T. Wang, J. Kingsley, A.R. Buckley, D.G. Lidzey, A.M. Donald, Grain size dependence of degradation of aluminium/calcium cathodes in organic solar cells following exposure to humid air, Sol. Energy Mater. Sol. Cells 140 (2015) 25–32.
[10] J. Adams, M. Salvador, L. Lucera, S. Langner, G.D. Spyropoulos, F.W. Fecher, M.M. Voigt, S.A. Dowland, A. Osvet, H.-J. Egelhaaf, C.J. Brabec, Water ingress in encapsulated inverted organic solar cells: correlating infrared imaging and photovoltaic performance, Adv. Energy Mater. 5 (2015) 1501065.
[11] M.S. White, D.C. Olson, S.E. Shaheen, N. Kopidakis, D.S. Ginley, Inverted bulk-heterojunction organic photovoltaic device using a solution-derived ZnO underlayer, Appl. Phys. Lett. 89 (2006) 143517.
[12] L.M. Chen, Z. Hong, G. Li, Y.R. Yang, Recent progress in polymer solar cells: manipulation of polymer:fullerene morphology and the formation of efficient inverted polymer solar cells, Adv. Mater. 21 (2009) 1434–1449.
[13] L. Derue, O. Dautel, A. Tournebize, M. Drees, H. Pan, S. Berthumeyrie, B. Pavageau, E. Cloutet, S. Chambon, L. Hirsch, A. Rivaton, P. Hudhomme, A. Facchetti, G. Wantz, Thermal stabilisation of polymer–fullerene bulk heterojunction morphology for efficient photovoltaic solar cells, Adv. Mater. 26 (2014) 5831–5838.
[14] R.Q. Png, P.J. Chia, J.C. Tang, B. Liu, S. Sivaramakrishnan, M. Zhou, S.H. Khong, H.S.O. Chan, J.H. Burroughes, L.L. Chua, R.H. Friend, P.K.H. Ho, High-performance polymer semiconducting heterostructure devices by nitrene-mediated photocrosslinking of alkyl side chains, Nat. Mater. 9 (2010) 152–158.
[15] C.P. Yau, S. Wang, N.D. Treat, Z. Fei, B.J. Tremolet de Villers, M.L. Chabinyc, M. Heeney, Investigation of radical and cationic cross-linking in high-efficiency, low band gap solar cell polymers, Adv. Energy Mater. 5 (2015) 1401228.
[16] G. Griffini, J.D. Douglas, C. Piliego, T.W. Holcombe, S. Turri, J.M.J. Fréchet, J.L. Mynar, Long-term thermal stability of high-efficiency polymer solar cells based on photocrosslinkable donor-acceptor conjugated polymers, Adv. Mater. 23 (2011) 1660–1664.
[17] S. Miyanishi, K. Tajima, K. Hashimoto, Stabilization of polymer photovoltaic cells by using cross-linkable poly(3-(5-hexenyl)thiophene, Macromolecules 42 (2009) 1610–1618.
[18] B.J. Kim, Y. Miyamoto, B. Ma, J.M.J. Fréchet, Photocrosslinkable polythiophenes for efficient, thermally stable, organic photovoltaics, Adv. Funct. Mater. 19 (2009) 2273–2281.
[19] C.-Y. Nam, Y. Qin, Y.S. Park, H. Hlaing, X. Lu, B.M. Ocko, C.T. Black, Photo-cross-linkable azide-functionalized polythiophene for thermally stable bulk heterojunction solar cells, Macromolecules 45 (2012) 2338–2347.
[20] H.J. Kim, A. Han, C.-H. Cho, H. Kang, H.H. Cho, M.Y. Lee, J.M.J. Fréchet, J.H. Oh, B.J. Kim, Solvent-resistant organic transistors and thermally stable organic photovoltaics based on cross-linkable conjugated polymers, Chem. Mater. 24 (2012) 215–221.
[21] F. Ouhib, M. Tomassetti, J. Manca, F. Piersimoni, D. Spoltore, S. Bertho, H. Moons, R. Lazzaroni, S. Desbief, C. Jerome, C. Detrembleur, Thermally stable bulk heterojunction solar cells based on cross-linkable acrylate-functionalized polythiophene diblock copolymers, Macromolecules 46 (2013) 785–795.
[22] Y.-J. Cheng, C.-H. Hsieh, P.-J. Li, C.-S. Hsu, Highly thermal stable and efficient organic photovoltaic cells with crosslinked networks appending open-cage fullerenes as additives, Adv. Funct. Mater. 21 (2011) 1723.
[23] B. Liu, R.Q. Png, L.H. Zhao, L.L. Chua, R.H. Friend, P.K. Ho, High internal quantum efficiency in fullerene solar cells based on crosslinked polymer donor networks, Nat. Commun. 3 (2012) 1321.
[24] C. Tao, M. Aljada, P.E. Shaw, K.H. Lee, H. Cavay, M.N. Balfour, R.J. Borthwick, M. James, P.L. Burn, I.R. Gentle, P. Meredith, Controlling hierarchy in solution--processed polymer solar cells based on crosslinked P3HT, Adv. Energy Mater. 3 (2013) 105–112.
[25] F. Huang, H.B. Wu, H.D.L. Wang, W. Yang, Y. Cao, Novel electroluminescent conjugated polyelectrolytes based on polyfluorene, Chem. Mater. 16 (2004) 708–716.
[26] H. Wu, F. Huang, Y. Mo, W. Yang, D. Wang, J. Peng, Y. Cao, Efficient electron injection from a bilayer cathode consisting of aluminum and alcohol-/water-soluble conjugated polymers, Adv. Mater. 16 (2004) 1826–1830.
[27] Z. He, C. Zhong, S. Su, M. Xu, H. Wu, Y. Cao, Enhanced power-conversion efficiency in polymer solar clls using an inverted device structure, Nat. Photon. 6 (2012) 591–595.
[28] K. Zhang, C. Zhong, S. Liu, C. Mu, Z. Li, H. Yan, F. Huang, Y. Cao, Highly efficient inverted polymer solar cells based on a crosslinkable water-/alcohol-aoluble conjugated polymer interlayer, ACS Appl. Mater. Interfaces 6 (2014) 10429–10435.
[29] Q. Hu, Y. Liua, Y. Lia, L. Yingc, T. Liua, F. Huangc, S. Wanga, W. Huangd, R. Zhua, Q. Gonga, Efficient and low-temperature processed perovskite solar cells based on a cross-linkable hybrid interlayer, J. Mater. Chem. 3 (2015) 18483–18491.
[30] K. Zhang, C. Zhong, S. Liu, A. Liang, S. Dong, F. Huang, High efficiency solution processed inverted white organic light emitting diodes with a cross-linkable amino-functionalized polyfluorene as a cathode interlayer, J. Mater. Chem. C 2 (2014) 3270–3277.
[31] Q. Hua, Y. Liua, Y. Lia, L. Ying, T. Liu, F. Huang, S. Wang, W. Huang, R. Zhu, Q. Gong, Efficient and low-temperature processed perovskite solar cells based on a cross-linkable hybrid interlayer, J. Mater. Chem. 3 (2015) 18483–18491.
[32] Z. Zhu, C.C. Chueh, G. Zhang, F. Huang, H. Yan, A.K.Y. Jen, Improved ambient-stable perovskite solar cells enabled by a hybrid polymeric electron-transporting layer, ChemSusChem 9 (2016) 1–7.
[33] Z. Zhu, Q. Xue, H. He, K. Jiang, Z. Hu, Y. Bai, T. Zhang, S. Xiao, K. Gundogdu, B.R. Gautam, H. Ade, F. Huang, K.S. Wong, H.L. Yip, S. Yang, H.A. Han, PCBM electron transport layer containing small amounts of dual polymer additives that enables enhanced perovskite solar cell performance, Adv. Sci. (2015) 1500353.
[34] H. Wang, C. Xie, W. Zhang, S. Cai, Z. Yang, Y. Gui, J. Hazard Mater. 141 (2007) 645–652.
[35] B. Fan, L. Ying, P. Zhu, F. Pan, F. Liu, J. Chen, F. Huang, Y. Cao, All-polymer solar cells based on a conjugated polymer containing siloxane-functionalized side chains with efficiency over 10%, Adv. Mater. 29 (2017) 1703906.
[36] B. Fan, L. Ying, Z. Wang, B. He, X.-F. Jiang, F. Huang, Y. Cao, Optimisation of processing solvent and molecular weight for the production of A green-solvent-processed all-polymer solar cells with a power conversion efficiency over 9%, Energy Environ. Sci. 10 (2017) 1243–1251.
[37] S. Kundu, S.R. Gollu, R. Sharma, G. Srinivas, A. Ashok, A. Kulkarni, D. Gupta, Device stability of inverted and conventional bulk heterojunction solar cells with MoO_3 and ZnO nanoparticles as charge transport layers, Org. Electron. 14 (2013) 3083–3088.
[38] X. Gu, W. Cui, H. Li, Z. Wu, Z. Zeng, S.T. Lee, H. Zhang, B.A. Sun, Solution-processed hole extraction layer made from ultrathin MoS2 nanosheets for efficient organic solar cells, Adv. Energy Mater. 3 (2013) 1262–1268.
[39] J. Bisquert, Theory of the impedance of electron diffusion and recombination in a thin layer, J. Phys. Chem. 106 (2002) 325–333.
[40] F.J. Lim, A. Krishnamoorthy, G.W. Ho, Device stability and light-soaking characteristics of high-efficiency Benzodithiophene – Thienothiophene copolymer-based inverted organic solar cells with F-TiO_x electron-transport layer, ACS Appl. Mater. Interfaces 7 (2015) 12119–12127.
[41] A. Gaur, P. Kumar, Studies on stability of Bi-functional P3HT:PCBM:rubrene optoelectronic devices, Appl. Phys. A 111 (2013) 877–886.
[42] S.M. Willis, C. Cheng, H.E. Assender, ans A.A.R. Watt, The transitional heterojunction behavior of PbS/ZnO colloidal quantum dot solar cells, Nano Lett. 12 (2012) 1522–1526.
[43] C.J. Schaffer, C.M. Palumbiny, M.A. Niedermeier, C. Jendrzejewski, G. Santoro, S.V. Roth, P.A. Müller-Buschbaum, Direct evidence of morphological degradation on a nanometer scale in polymer solar cells, Adv. Mater. 25 (2013) 6760–6764.
[44] W. Ostwald, Lehrbuch der Allgemeinen Chemie 2 (1896) Part 1.
[45] W. Zhao, D. Qian, S. Zhang, S. Li, O. Inganäs, F. Gao, J. Hou, Fullerene-free polymer solar cells with over 11% efficiency and excellent thermal stability, Adv. Mater. 28 (2016) 4734–4739.
[46] J.M. Szarko, J. Guo, Y. Liang, B. Lee, B.S. Rolczynski, J. Strzalka, T. Xu, S. Loser, T.J. Marks, L. Yu, L.X. Chen, When function follows form: effects of donor copolymer side chains on film morphology and BHJ solar cell performance, Adv. Mater. 22 (2010) 5468–5472.
[47] Y. Zhang, Y. Xu, M.J. Ford, F. Li, J. Sun, X. Ling, Y. Wang, J. Gu, J. Yuan, W. Ma, Thermally stable All-polymer solar cells with high tolerance on blend ratios, Adv. Energy Mater. 8 (2018) 1800029.